

Detecting Non-Markovianity via Quantified Coherence: Theory and Experiments

Kang-Da Wu,^{1,2} Zhibo Hou,^{1,2} Guo-Yong Xiang,^{1,2,*} Chuan-Feng Li,^{1,2} Guang-Can Guo,^{1,2} Daoyi Dong,³ and Franco Nori^{4,5}

¹CAS Key Laboratory of Quantum Information, University of Science and Technology of China, Hefei, 230026, People's Republic of China

²CAS Center For Excellence in Quantum Information and Quantum Physics,

University of Science and Technology of China, Hefei, 230026, People's Republic of China

³School of Engineering and Information Technology, University of New South Wales, Canberra, ACT, 2600, Australia

⁴Theoretical Quantum Physics Laboratory, RIKEN Cluster for Pioneering Research, Wako-shi, Saitama 351-0198, Japan

⁵Physics Department, University of Michigan, Ann Arbor Michigan 48109-1040, USA

(Dated: March 11, 2019)

The dynamics of open quantum systems and manipulation of quantum resources are both of fundamental interest in quantum physics. Here, we investigate the relation between quantum Markovianity and coherence, providing an effective way for detecting non-Markovianity based on the *quantum-incoherent relative entropy of coherence* (*QI REC*). We theoretically show the relation between completely positive (CP) divisibility and the monotonic behavior of the *QI REC*. Also we implement an all-optical experiment to demonstrate that the behavior of the *QI REC* is coincident with the entanglement shared between the system and the ancilla for both Markovian and non-Markovian evolution; while other coherence-based non-Markovian information carriers violate monotonicity, even in Markovian processes. Moreover, we experimentally observe that non-Markovianity enhances the ability of creating coherence on an ancilla. This is the first experimental study of the relation between dynamical behavior of the *QI REC* and the phenomenon of information backflow. Moreover, our method for detecting non-Markovianity is applicable to general quantum evolutions.

I. INTRODUCTION

Quantum resource theory [1] studies the transformation and conversion of information under certain constraints, the quantification and manipulation of various resources are of central interest in quantum information, quantum thermodynamics, and other fields of physics [2–5]. Recently, resource theories have inspired rigorous studies on the long-standing notions of non-classicality in localized systems, where the development of coherence theory has become a fundamental task [6–11].

Coherence is an intrinsically vulnerable resource, inevitably vanishing at macroscopic scales of space, time, and temperature [12–17]. This becomes apparent in the study of the dynamical behavior of such resource in the presence of dissipation, where the system is rarely isolated and usually loses its information due to its environment [18–26]. The problem of classifying memoryless dynamics and dynamics exhibiting memory effects has stimulated numerous investigations on the system-environment interaction. There are two main ideas: one idea, based on divisibility of the dynamical maps [27, 28], is an analogy with the definition of classical stochastic processes; the other idea [29] demonstrates that the memory effects may be accompanied with an information backflow, which is reflected by the non-monotonic behavior of some physical quantities [29–42].

Rigorous studies on the dynamical behavior of quantified coherence in the presence of non-Markovian

noise have recently attracted considerable attention [43–53]. Moreover, information quantifiers based on coherence and the extended coherence with an ancilla have been proposed, for measuring the degree of non-Markovianity. It is known that coherence behaves monotonically in an incoherent Markovian evolution. However, for a general Markovian evolution, the dynamical behavior of quantum coherence is not necessarily monotonic. Moreover, the coherence-based quantifier that evolves monotonically in a certain basis may not evolve monotonically in another basis. Thus, two basic requirements for an advantageous coherence-based non-Markovianity measures are: (a) it is applicable for general evolutions; (b) for a Markovian quantum evolution, the monotonicity of the dynamical behavior of the quantifier is independent of the choice of reference basis.

In this work, we introduce a new way for detecting non-Markovianity based on the *QI REC* of a bipartite system [54–56]. Theoretically, we show that Markovianity implies the monotonic behavior of both the *QI REC* and the *steering-induced coherence* (SIC, upper bounded by the *QI REC*) [55, 56]. Experimentally, we compare our method with two existing approaches [43, 45], and verify the advantages of our new method for characterizing non-Markovianity. Moreover, we experimentally detect non-Markovianity via the non-monotonic behavior of both the *QI REC* and the SIC, which is coincident with previous results based on entanglement. Our work links the resource theory of coherence to quantum Markovianity.

* gyxiang@ustc.edu.cn

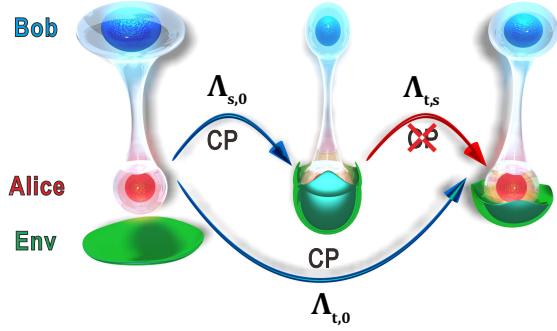


Figure 1. **Theoretical Framework.** Consider a bipartite system involving Alice (red, system) and Bob (blue, ancilla) with nonzero initial QI REC, which is shown by the bigger volume of Bob. The environment is shown as green and can interact with Alice’s system, while Bob is immune to the environment. Then Alice undergoes a quantum evolution which can be characterized by a family of t -parameterized dynamical maps $\{\Lambda_t\}$. If the evolution is CP divisible, then QI REC decreases monotonically. The CPTP map on Alice’s system also affects the ability of preparing coherent states on Bob’s system, in both the asymptotic limit and single-shot regimes (this is shown by the behavior of the SIC, and theoretically proved in the Supplementary Materials), which is shown by the decrease of Bob’s volume. However, any temporal increase of the QI REC or the SIC indicates the violation of CPTP of the intermediate map $\Lambda_{t,s}$, and non-Markovianity.

II. THEORY

First we describe the theoretical framework in an abstract fashion, including a brief introduction to quantum Markovianity, quantification of coherence, and its relation to non-Markovianity.

Quantum Markovianity—In general, quantum evolution can be characterized by a family of one-parameter dynamical maps $\{\Lambda_{t,0}\}$ ($\Lambda_{t,0}$ is completely positive and trace preserving (CPTP) for any $t > 0$, i.e., a legitimate quantum operation that maps the initial quantum state to the state at time t) and we assume that the inverse $\Lambda_{t,0}^{-1}$ exists for all time $t > 0$. Thus, for any $t > s > 0$, we can write the dynamical map for any t into a composition

$$\Lambda_{t,0} = \Lambda_{t,s}\Lambda_{s,0}. \quad (1)$$

However, even though Λ_t^{-1} is well-defined and $\Lambda_{t,0}$, $\Lambda_{s,0}$ are completely positive (CP), the map $\Lambda_{t,s}$ does not need to be CP. If for any $t > s > 0$, $\Lambda_{t,s}$ is CP, then the family of dynamical maps is said to be CP divisible. This leads to the definition of quantum Markovianity, providing a mathematical characterization of a map describing a memoryless evolution as a composition of physical maps. In this paper we adopt CP divisibility as the essential property of quantum Markovianity.

Quantum-incoherent relative entropy of coherence—In the resource theory of coherence, an orthogonal basis $\{|i\rangle\}$

is considered classical. Any mixture of such states is termed *incoherent*. And *incoherent operations* are naturally introduced as physical transformations that do not create coherence [7].

The amount of coherence for a general quantum state quantifies how close it is from the set of incoherent states with respect to a given reference basis, i.e., $C_r \equiv \min_{\chi \in \mathcal{I}} S(\rho \| \chi)$, where $S(\rho \| \chi) = \text{Tr}[\rho \log_2 \rho - \rho \log_2 \chi]$ denotes the quantum relative entropy [59], and \mathcal{I} denotes the set of incoherent states.

Strictly, C_r never increases under CPTP incoherent operations. However, when taking the advantage of assistance [54, 60], one can increase C_r . Considering a bipartite system (Alice and Bob), assume Alice can perform any local projective measurement on her system and broadcast the outcomes to Bob. Then Bob can prepare more coherent states than his own states. In particular, the SIC [55, 56] is defined as the maximal average coherence on Bob’s side, $\bar{C}_r^B(\rho^{AB}) = \max_{\mathcal{M}_A} \sum_m p_m C_r(\rho_m^B)$, where the optimization is taken over all projective measurements \mathcal{M}_A on Alice and ρ_m is the state corresponding to the measurement outcome m .

The SIC captures the steerability from Alice to Bob, where coherence on Bob’s side is demanded. Generally, the identification of the SIC needs a non-trivial optimization over all possible measurements of Alice. The upper bound of this quantity, the QI REC was recently introduced in [54, 60],

$$C_r^{AB}(\rho^{AB}) \equiv \min_{\chi^{AB} \in \mathcal{I}^{AB}} S(\rho^{AB} \| \chi^{AB}), \quad (2)$$

where χ^{AB} denotes the bipartite states that are *quantum-incoherent (QI)*; i.e., $\chi^{AB} = \sum_i p_i \sigma_i^A \otimes |i\rangle\langle i|^B$, where σ_i^A represents an arbitrary quantum state, belonging to Alice. Note that the QI REC is a measure that is different from entanglement or correlation measure (see the Supplementary Material for details on the QI REC).

Non-Markovianity witness via the QI REC—The theoretical framework is shown in Fig. 1. Considering the aforementioned bipartite system and assuming Alice will interact with her environment while Bob is kept isolated, then we have the following results.

Theorem 1—In a bipartite state (Alice and Bob), assume that Alice undergoes an evolution characterized by $\{\Lambda_{t,0}\}$. Then the QI REC decreases monotonically if $\{\Lambda_{t,0}\}$ is CP divisible, i.e., for any $t > s > 0$,

$$C_r^{AB}(\rho_s^{AB}) \geq C_r^{AB}(\rho_t^{AB}), \quad (3)$$

where ρ_s^{AB} and ρ_t^{AB} are the states after the evolution times s and t , respectively. Moreover, the SIC decreases monotonically if $\{\Lambda_{t,0}\}$ is Markovian.

The result demonstrates that the QI REC on Bob’s side provides a new method for characterizing the CP divisibility of a general quantum process on Alice’s side. And the violation of monotonic behavior of either the QI REC or the SIC indicates non-Markovianity. The proof is presented in the Supplementary Material.

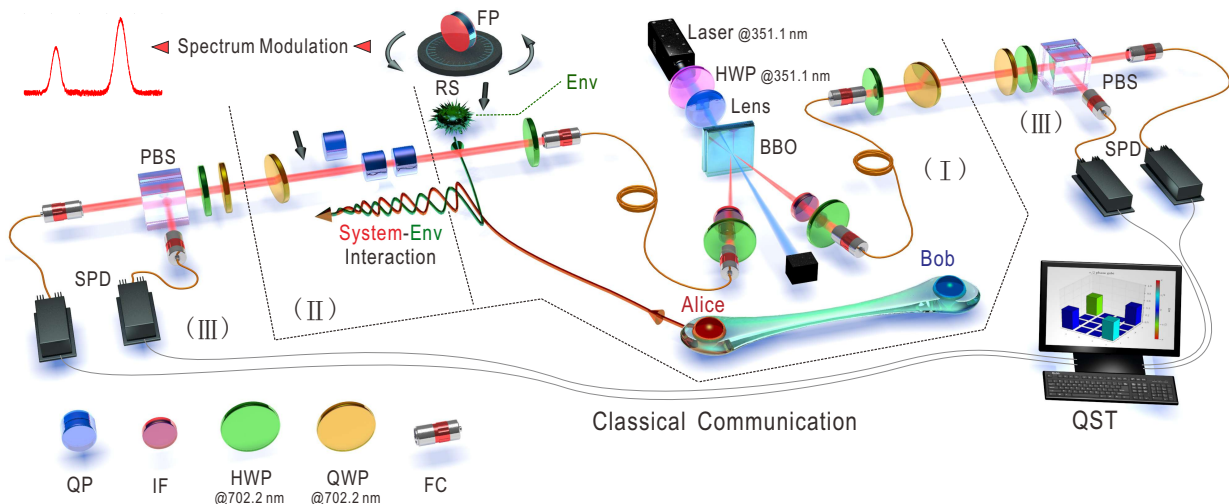


Figure 2. The experimental setup is constructed by three modules: (I) state preparation, (II) evolution, and (III) detection. In (I), we can prepare two-photon states $\cos 2\theta|00\rangle + \sin 2\theta|11\rangle$, with arbitrary θ and $0 \equiv H$ and $1 \equiv V$. The environmental state can be modified by inserting a Fabry-Pérot cavity [57]. In (II), the polarization and frequency degrees of freedom are coupled in a quartz plate (QP) in which different evolution times are realized by varying the thickness of the plates. The angles of the QPs can be controlled for dephasing in an arbitrary basis. Without modifying the spectrum of the frequency of Alice's photons, the environmental state can be modeled as a Gaussian distribution, resulting in a Markovian evolution of Alice's system. With the FP cavity (with thickness $h \approx 0.06$ mm, and partial reflecting coating on each side) inserted, the environmental state of Alice can be modeled by the sum of two Gaussians centered at two different frequencies. In (III), the overall two-qubit quantum state ρ_t^{AB} and a single-qubit state ρ_t^A (on Alice's side) at different evolution times t can be analyzed. Thus, we can obtain the experimental values for relevant information quantifiers. The coherence-based measures in different reference bases can be experimentally obtained for comparison. This setup can also be used for performing a local projective measurement on Alice and broadcasting the outcomes to Bob [58], which can experimentally detect the SIC. Keywords include: IF, interference filter; HWP, half-wave plate; QWP, quarter-wave plate; QP, quartz plate; FP, Fabry-Pérot cavity; BBO, β -barium borate; SPD, single photon detector; FC, fiber coupler; PBS, polarizing beam splitter; Env, environment; QST, quantum state tomography.

III. EXPERIMENTS

In our experiments, the system-environment interaction is provided by the coupling of the polarization degree (Alice, the open system) and frequency degree (environment) of Alice's photons. The experimental setup is illustrated in Fig. 2, and is constructed by three modules (for more information, see the Supplementary Materials).

Our experiments contain two parts. In the first part, we implement a monotonicity test. In particular, we rotate the angles of all QPs to 20° , producing a pure decoherence in the eigenbasis of $\sigma \cdot n_0$ on Alice, where $n_0 = \cos 2\theta e^X + \sin 2\theta e^Z$ and $\theta = 20^\circ$, maximizing the non-monotonic behavior of the extended coherence and the local coherence. We prepare both a Bell state $|\psi\rangle^{AB}$ (shared by Alice and Bob) and an incoherent pure state $|0\rangle^A$. Then we obtain the concurrence $E_c^{AB}(\rho_t^{AB})$, the QI REC, the extended coherence, and the local coherence at various evolution times t . The experimental values for the above quantifiers are shown as black diamonds, blue squares, purple up-triangles and red disks in Fig. 3(a), with respect to the eigenbasis of $\sigma_z^A \otimes \sigma_z^B$. The experimental dynamics for the QI REC, the extended coherence and the local coherence with respect to different bases are

also shown in Figs. 3(b-d), respectively. From these results, we can see that both the behaviors of the extended coherence and the local coherence are non-monotonic and basis-dependent; only the QI REC behaves monotonically during the Markovian process.

In the second part of the experiment, we implement a quantum evolution that is non-Markovian, for exploring the behaviors of the QI REC and the SIC in the presence of non-Markovian system-environment interactions. Since either the extended coherence or the local coherence behaves non-monotonically even in a Markovian process, we do not show them in the second part of the experiments. The evolution is constructed as decoherence in the σ_z basis. We insert a Fabry-Pérot cavity into Alice's path, resulting in a modification of the spectrum of the frequency of Alice's photons. At different evolution times t , the values for concurrence and the QI REC (with respect to different bases) are obtained. The relevant experimental values are shown as black diamonds and blue squares in Figs. 4(a, b). The dynamical behaviors of the SIC and the local coherence of Bob $C_r^B(\rho_t^B)$ are also investigated (in the σ_z^B basis) and shown as green down-triangles and pink disks in Fig. 5(a). And the evolution of the optimal steered states are shown in Fig. 5(b). It is clear that the non-Markovianity can be

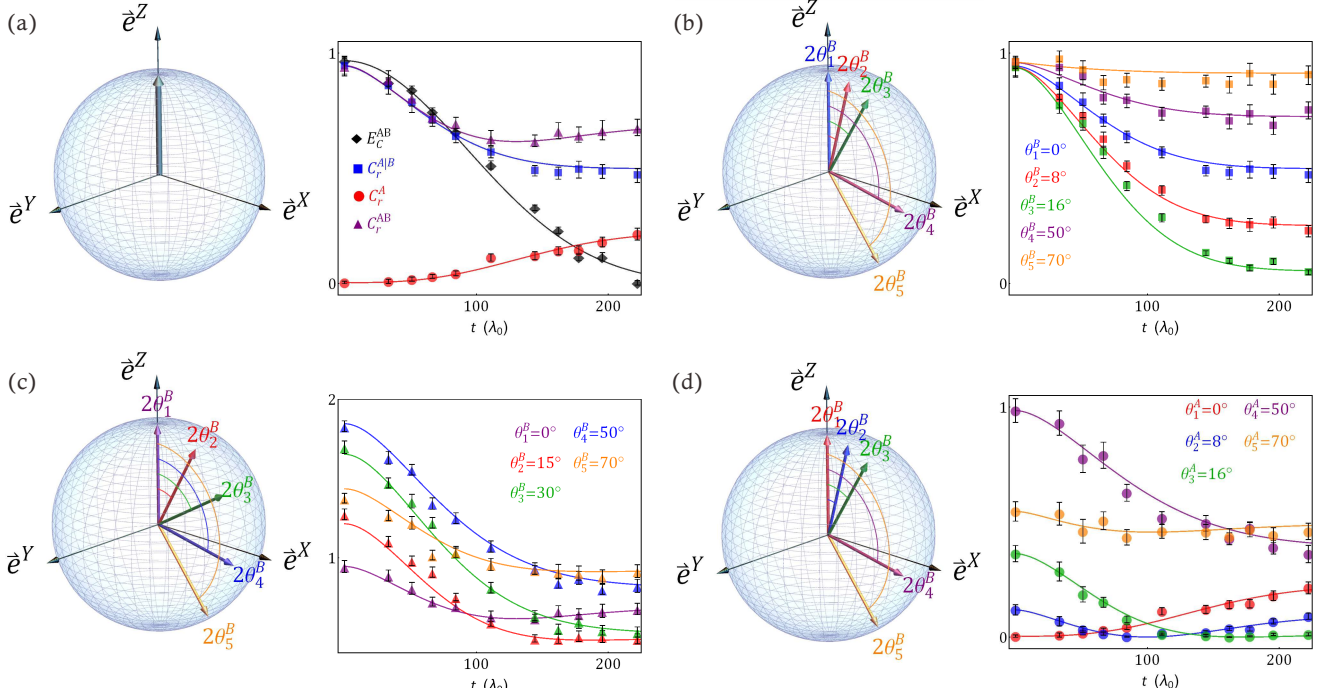


Figure 3. **Experimental Results for monotonicity testing.** The Markovian evolution is constructed as decoherence in the eigenbasis of $\sigma \cdot n_0$, where $n_0 = \cos 40^\circ e^X + \sin 40^\circ e^Z$ and $\sigma = (\sigma_x, \sigma_y, \sigma_z)$, by setting the rotation angle of the QPs to 20° . The evolution is implemented on both: a single system (Alice is prepared in $|0\rangle$) and a bipartite system (Alice and Bob initially share a maximally entangled state $|\phi\rangle^{AB}$). In (a), the experimental values for the concurrence, the QI REC, the extended coherence (with respect to the eigenbasis of $\sigma_z^A \otimes \sigma_z^B$), and the local coherence of Alice (with respect to the σ_z^A basis) are shown as black diamonds, blue squares, purple up-triangles, and red disks, respectively. The dynamical behaviors of these coherence quantifiers are also tested with respect to different bases. The experimental values for the QI REC, the extended coherence, and the local coherence with respect to different bases are also obtained and shown in (b-d), respectively. For the QI REC, we choose five reference bases as the eigenbasis of $\sigma_z^A \otimes [\sigma \cdot n(\theta_i^B)]$, where $n(\theta_i^B) = \sin 2\theta_i^B e^X + \cos 2\theta_i^B e^Z$, and $i=1-5$. The values of θ_i^B are shown in (b). In the right of (b), squares in different colors show the dynamical behavior of the QI REC in different bases. For the extended coherence, the different reference bases are also chosen as eigenbasis of $\sigma_z^A \otimes [\sigma \cdot n(\theta_i^B)]$ for various θ_i^B . For the local coherence, five different bases of Alice are chosen according to the eigenbasis of $\sigma \cdot n(\theta_i^A)$. The choices of $\theta_i^{A(B)}$ are shown in the corresponding sub figures. All solid lines represent numerical simulations considering the fidelity of the states prepared in our laboratory, deduced assuming that the spectrum of Alice's photon is a Gaussian profile with a FWHM of 4 nm.

captured by both the QI REC and the SIC.

All solid lines represent numerical simulations considering the experimental imperfections. In the Supplementary Material, we show that the experimental results admit a theoretical analysis, and we also perform numerical simulations to show that both the QI REC and the SIC are applicable to a large range of quantum processes for witnessing non-Markovianity.

IV. DISCUSSION

In this work, we theoretically provided a method for characterizing Markovianity based on the QI REC (between an open system and an ancilla) and experimentally investigated the evolution of the local coherence, the extended coherence, the QI REC, and the SIC in both Markovian and non-Markovian processes. We highlight the two-fold advantages of our method: on the one

hand, it overcomes the constraint in [43, 45, 49] as it can be applied to general quantum evolutions; on the other hand, the information carrier based on QI REC does not need any non-trivial optimization. Moreover, in the experiments with the non-Markovian processes, these results show that the information backflow can enhance the ability of preparing coherent states on the ancilla system, in both asymptotic and single-shot settings, linking non-Markovianity to quantum resource theory.

A full understanding of these connections still remains open. Quantum coherence has been regarded as a type of resource which is more fundamental than quantum correlations, and current researches highlight the links between different quantum resources [61–63]. Though relatively elegant solutions come up in the context of coherence and correlations, a natural question arises that whether there exists a construction for the links between general quantum resources and non-Markovianity.

Another promising line of research is studying the dy-

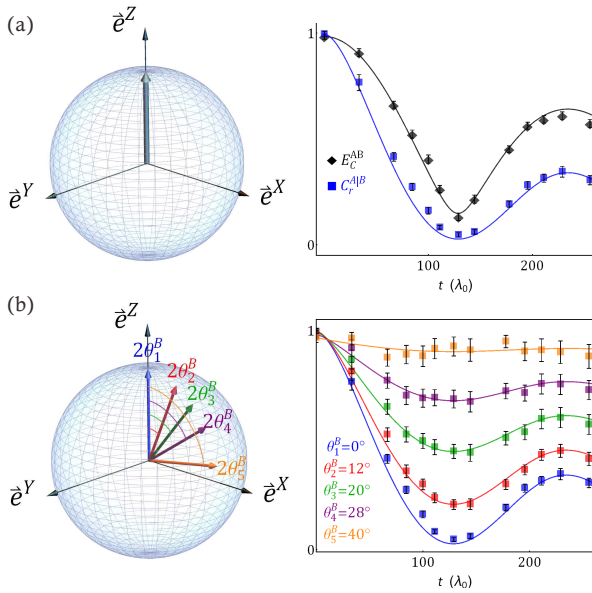


Figure 4. **Experimental results for detecting non-Markovianity via QI REC.** The evolution is constructed as pure decoherence in the σ_z basis. The experimental values for the concurrence and the QI REC (with respect to the eigenbasis of $\sigma_z^A \otimes \sigma_z^B$) at different evolution times t are shown as black diamonds and blue squares in (a). For the QI REC, four different bases are chosen according to the eigenbasis of $\sigma_z^A \otimes [\sigma \cdot \mathbf{n}(\theta_i^B)]$ with different θ_i^B . All solid lines represent numerical simulations considering experimental imperfections, which are deduced assuming that the spectrum of Alice's photon is a sum of two Gaussians centered at two different frequencies, corresponding to wavelengths 700.6 nm and 703.3 nm with amplitudes 0.65 and 0.35.

namics of resource conversion processes. It has been put forward that utilizing correlated resources, together with measurement feed-forward, can be advantageous in implementing certain gates in measurement-based computation [64]. If the non-Markovianity could be related to enhancing the operational advantages of such protocols, it could imply that operational benefits can emerge when information backflow takes place.

The work at USTC is supported by the National Natural Science Foundation of China under Grants (Nos. 11574291, 11774334, and 61828303), the National Key Research and Development Program of China (No.2017YFA0304100), Key Research Program of Frontier Sciences, CAS (No.QYZDY-SSW-SLH003), National Key R & D Program (2016YFA0301700), and Anhui Initiative in Quantum Information Technologies. D.D. acknowledges partial support by the Australian Research Council's Discovery Projects Funding Scheme under Project DP190101566.

-
- [1] F. G. S. L. Brandão and G. Gour, *Phys. Rev. Lett.* **115**, 070503 (2015).
- [2] G. Gour, I. Marvian, and R. W. Spekkens, *Phys. Rev. A* **80**, 012307 (2009).
- [3] I. Marvian and R. W. Spekkens, *Nat. Commun.* **5**, 3821 (2014).
- [4] F. G. S. L. Brandão, M. Horodecki, J. Oppenheim, J. M. Renes, and R. W. Spekkens, *Phys. Rev. Lett.* **111**, 250404 (2013).
- [5] M. Lostaglio, K. Korzekwa, D. Jennings, and T. Rudolph, *Phys. Rev. X* **5**, 021001 (2015).
- [6] A. Streltsov, G. Adesso, and M. B. Plenio, *Rev. Mod. Phys.* **89**, 041003 (2017).
- [7] T. Baumgratz, M. Cramer, and M. B. Plenio, *Phys. Rev. Lett.* **113**, 140401 (2014).
- [8] D. Girolami, *Phys. Rev. Lett.* **113**, 170401 (2014).
- [9] A. Streltsov, U. Singh, H. S. Dhar, M. N. Bera, and G. Adesso, *Phys. Rev. Lett.* **115**, 020403 (2015).
- [10] A. Winter and D. Yang, *Phys. Rev. Lett.* **116**, 120404 (2016).
- [11] X. Yuan, H. Zhou, Z. Cao, and X. Ma, *Phys. Rev. A* **92**, 022124 (2015).
- [12] T. R. Bromley, M. Cianciaruso, and G. Adesso, *Phys. Rev. Lett.* **114**, 210401 (2015).
- [13] I. A. Silva, A. M. Souza, T. R. Bromley, M. Cianciaruso, R. Marx, R. S. Sarthour, I. S. Oliveira, R. L. Franco, S. J. Glaser, E. R. deAzevedo, D. O. Soares-Pinto, and G. Adesso, *Phys. Rev. Lett.* **117**, 160402 (2016).
- [14] Z. Huang and H. Situ, *Quantum Inf. Process.* **16**, 222 (2017).
- [15] M. Qin, Z. Ren, and X. Zhang, *Phys. Rev. A* **98**, 012303 (2018).
- [16] M. Lostaglio, K. Korzekwa, and A. Milne, *Phys. Rev. A* **96**, 032109 (2017).
- [17] Z.-X. Man, Y.-J. Xia, and R. L. Franco, *Sci. Rep.* **5**, 13843 (2015).
- [18] H.-P. Breuer and F. Petruccione, *The Theory of Open Quantum Systems* (Oxford University Press on Demand, 2002).
- [19] U. Weiss, *Quantum Dissipative Systems*, Vol. 13 (World scientific, 2012).
- [20] W.-M. Zhang, P.-Y. Lo, H.-N. Xiong, M. W.-Y. Tu, and F. Nori, *Phys. Rev. Lett.* **109**, 170402 (2012).
- [21] Y.-N. Chen, G.-Y. Chen, Y.-Y. Liao, N. Lambert, and F. Nori, *Phys. Rev. B* **79**, 245312 (2009).
- [22] X. Yin, J. Ma, X. Wang, and F. Nori, *Phys. Rev. A* **86**, 012308 (2012).
- [23] J. Zhang, Y.-X. Liu, R.-B. Wu, K. Jacobs, and F. Nori, *Phys. Rev. A* **87**, 032117 (2013).
- [24] H.-B. Chen, N. Lambert, Y.-C. Cheng, Y.-N. Chen, and

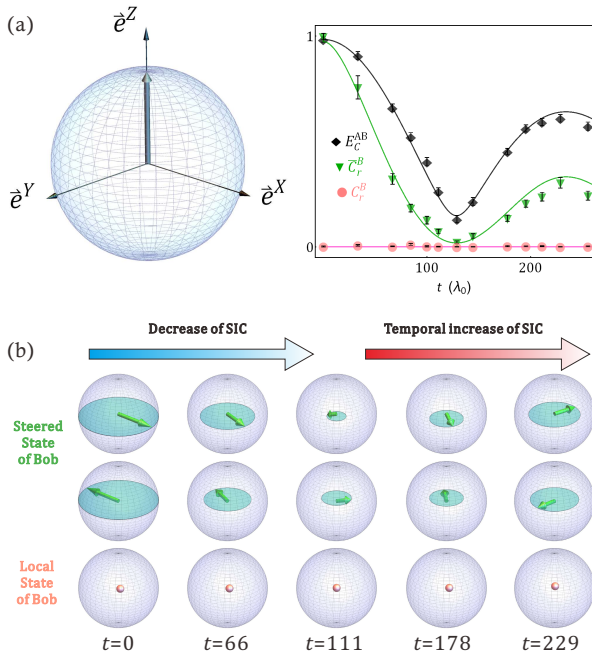


Figure 5. **Experimental results for detecting Non-Markovianity via SIC.** The dynamical behavior of the SIC (in the σ_z^B basis) was also investigated under the aforementioned evolution. The experimental values are shown in (a). In the presence of the non-Markovian decoherence noise, the optimal measurement on Alice's system is σ_x^A measurement on Alice. (b) illustrates the dynamical behavior of the SIC with respect to the σ_z^B basis. The assisted state conversion process consists of a σ_x^A measurement and the broadcast of outcomes 0 or 1 to Bob. Bob then can prepare a more coherent state at each time t . Bob's two steered states and local states are shown as Bloch vectors in green and pink respectively, and the radius of the disks $R(t) = \sqrt{r_x(t)^2 + r_y(t)^2}$ show the coherence of each state. The experimental values for the local coherence on Bob's system are shown in (a) as pink disks.

F. Nori, *Sci. Rep.* **5**, 12753 (2015).

- [25] H.-N. Xiong, P.-Y. Lo, W.-M. Zhang, F. Nori, *et al.*, *Sci. Rep.* **5**, 13353 (2015).
- [26] F. A. Pollock, C. Rodríguez-Rosario, T. Frauenheim, M. Paternostro, and K. Modi, *Phys. Rev. Lett.* **120**, 040405 (2018).
- [27] V. Gorini, A. Kossakowski, and E. C. G. Sudarshan, *J. Math. Phys.* **17**, 821 (1976).
- [28] G. Lindblad, *Commun. Math. Phys.* **48**, 119 (1976).
- [29] H.-P. Breuer, E.-M. Laine, and J. Piilo, *Phys. Rev. Lett.* **103**, 210401 (2009).
- [30] A. Rivas, S. F. Huelga, and M. B. Plenio, *Phys. Rev. Lett.* **105**, 050403 (2010).
- [31] X.-M. Lu, X. Wang, and C. P. Sun, *Phys. Rev. A* **82**, 042103 (2010).
- [32] H. Song, S. Luo, and Y. Hong, *Phys. Rev. A* **91**, 042110 (2015).
- [33] A. K. Rajagopal, A. R. Usha Devi, and R. W. Rendell, *Phys. Rev. A* **82**, 042107 (2010).
- [34] S. Luo, S. Fu, and H. Song, *Phys. Rev. A* **86**, 044101 (2012).
- [35] B. Bylicka, D. Chruściński, and S. Maniscalco, *Sci. Rep.* **4**, 5720 (2014).
- [36] S. Lorenzo, F. Plastina, and M. Paternostro, *Phys. Rev. A* **88**, 020102 (2013).
- [37] J. Bae and D. Chruściński, *Phys. Rev. Lett.* **117**, 050403 (2016).
- [38] S.-L. Chen, N. Lambert, C.-M. Li, A. Miranowicz, Y.-N. Chen, and F. Nori, *Phys. Rev. Lett.* **116**, 020503 (2016).
- [39] A. Strathearn, P. Kirton, D. Kilda, J. Keeling, and B. W. Lovett, *Nat. Commun.* **9**, 3322 (2018).
- [40] H.-Y. Ku, S.-L. Chen, H.-B. Chen, N. Lambert, Y.-N. Chen, and F. Nori, *Phys. Rev. A* **94**, 062126 (2016).
- [41] S.-J. Xiong, Y. Zhang, Z. Sun, L. Yu, Q. Su, X.-Q. Xu, J.-S. Jin, Q. Xu, J.-M. Liu, K. Chen, *et al.*, *Optica* **4**, 1065 (2017).
- [42] C.-M. Li, Y.-N. Chen, N. Lambert, C.-Y. Chiu, and F. Nori, *Phys. Rev. A* **92**, 062310 (2015).
- [43] Z. He, H.-S. Zeng, Y. Li, Q. Wang, and C. Yao, *Phys. Rev. A* **96**, 022106 (2017).
- [44] C. Radhakrishnan, P.-W. Chen, S. Jambulingam, T. Byrnes, M. Ali, *et al.*, arXiv:1711.03299 (2017).
- [45] T. Chanda and S. Bhattacharya, *Ann. Phys.* **366**, 1 (2016).
- [46] S. Y. Mirafzali and H. R. Baghshahi, *Physica A: Statistical Mechanics and its Applications* **514**, 274 (2019).
- [47] Y.-J. Zhang, W. Han, Y.-J. Xia, Y.-M. Yu, and H. Fan, *Sci. Rep.* **5**, 13359 (2015).
- [48] C. Addis, G. Brebner, P. Haikka, and S. Maniscalco, *Phys. Rev. A* **89**, 024101 (2014).
- [49] M. H. M. Passos, P. C. Obando, W. F. Balthazar, F. M. Paula, J. A. O. Huguenin, and M. S. Sarandy, arXiv:1807.05378 (2018).
- [50] Z.-X. Man, Y.-J. Xia, and R. L. Franco, *Physical Review A* **97**, 062104 (2018).
- [51] B. Çakmak, M. Pezzutto, M. Paternostro, and Ö. Müstecaplıoğlu, *Physical Review A* **96**, 022109 (2017).
- [52] Y. Liu, H.-M. Zou, and M.-F. Fang, arXiv preprint arXiv:1811.01154 (2018).
- [53] S. Bhattacharya, S. Banerjee, and A. K. Pati, Preprint at <https://arxiv.org/abs/1601.04742> (2016).
- [54] E. Chitambar, A. Streltsov, S. Rana, M. N. Bera, G. Adesso, and M. Lewenstein, *Phys. Rev. Lett.* **116**, 070402 (2016).
- [55] X. Hu and H. Fan, *Sci. Rep.* **6** (2016).
- [56] X. Hu, A. Milne, B. Zhang, and H. Fan, *Sci. Rep.* **6**, 19365 (2016).
- [57] B.-H. Liu, L. Li, Y.-F. Huang, C.-F. Li, G.-C. Guo, E.-M. Laine, H.-P. Breuer, and J. Piilo, *Nat. Phys.* **7**, 931 (2011).
- [58] K.-D. Wu, Z. Hou, H.-S. Zhong, Y. Yuan, G.-Y. Xiang, C.-F. Li, and G.-C. Guo, *Optica* **4**, 454 (2017).
- [59] V. Vedral, *Rev. Mod. Phys.* **74**, 197 (2002).
- [60] A. Streltsov, S. Rana, M. N. Bera, and M. Lewenstein, *Phys. Rev. X* **7**, 011024 (2017).
- [61] A. Streltsov, U. Singh, H. S. Dhar, M. N. Bera, and G. Adesso, *Phys. Rev. Lett.* **115**, 020403 (2015).
- [62] J. Ma, B. Yadin, D. Girolami, V. Vedral, and M. Gu, *Phys. Rev. Lett.* **116**, 160407 (2016).
- [63] K.-D. Wu, Z. Hou, Y.-Y. Zhao, G.-Y. Xiang, C.-F. Li, G.-C. Guo, J. Ma, Q.-Y. He, J. Thompson, and M. Gu, *Phys. Rev. Lett.* **121**, 050401 (2018).
- [64] R. Raussendorf and H. J. Briegel, *Phys. Rev. Lett.* **86**, 5188 (2001).
- [65] V. Vedral and M. B. Plenio, *Phys. Rev. A* **57**, 1619 (1998).
- [66] H. Ollivier and W. H. Zurek, *Phys. Rev. Lett.* **88**, 017901 (2001).
- [67] L. Henderson and V. Vedral, *J. Phys. A* **34**, 6899 (2001).
- [68] K. Modi, A. Brodutch, H. Cable, T. Paterek, and V. Vedral, *Rev. Mod. Phys.* **84**, 1655 (2012).

Appendix A: Theoretical tools

A *quantum resource theory* (QRT) has several indispensable ingredients, including: constraints, states which contain no resource, and the measure for how much resource that a state possesses. The constraints, known as free operations, in a QRT are often desirable from a practical perspective that reflects current experimental capabilities. The states that contain no resource are often referred to as free states, and these can be generated by free operations without any cost. In the following, let us first briefly recall some basic information about free states and free operations in coherence theory.

1. Free states in the resource theory of quantum coherence

The free states in the resource theory of quantum coherence are incoherent states [7]. A quantum state ρ is said to be incoherent in a given reference basis $\{|i\rangle\}$ if that state is diagonal in this basis, i.e.,

$$\rho = \sum_i p_i |i\rangle\langle i|, \quad (\text{A1})$$

where $0 \leq p_i \leq 1$ for all i , and $\sum_i p_i = 1$. The reference basis is often chosen according to the context of the story, usually motivated by physical grounds of being easy to synthesize or store, e.g., eigenbasis of the Hamiltonian in quantum thermodynamics, polarization or path degree of a photon, internal states of an ionic atom, and so on.

For bipartite systems partitioned by A and B , each with respective local reference bases $\{|i\rangle^A\}$ and $\{|j\rangle^B\}$, the incoherent states take the form

$$\chi^{AB} = \sum_{ij} p_{ij} |i\rangle\langle i|^A \otimes |j\rangle\langle j|^B, \quad (\text{A2})$$

where $0 \leq p_{ij} \leq 1$, and $\sum_{ij} p_{ij} = 1$. Note that in the aforementioned bipartite systems, we can also choose an orthogonal complete set of entangled pure states as the reference basis. In this case, the bipartite systems are viewed as a single physical system.

In the above case, coherence in both A and B are viewed as resources. In the task of *assisted distillation of quantum coherence* [54], involving a bipartite system (Alice and Bob) where only the coherence of Bob is viewed as a resource, the *quantum-incoherent (QI)* states are introduced and can be regarded as free states,

$$\chi^{AB} = \sum_i p_i \sigma_i^A \otimes |i\rangle\langle i|^B. \quad (\text{A3})$$

Here, σ_i^A is an arbitrary quantum state on Alice's side and the state $|i\rangle^B$ belongs to the local incoherent basis of Bob.

2. Quantification of quantum coherence in single and bipartite systems

Several coherence measures have been proposed, for quantifying the degree of coherence in both single systems and bipartite systems.

Regarding the degree of coherence in a single system, we adopt the most popular quantifier: the *relative entropy of coherence* (REC). The REC captures how far a given state ρ is from the set of incoherent states,

$$C_r(\rho) = \min_{\chi \in \mathcal{I}} S(\rho \| \chi), \quad (\text{A4})$$

where $S(\rho \| \chi)$ denotes the *relative entropy* between two quantum states ρ and χ ,

$$S(\rho \| \chi) = \text{Tr}(\rho \log_2 \rho - \rho \log_2 \chi), \quad (\text{A5})$$

and the minimization in Eq. (A4) is taken over all incoherent states. Another representation of REC is

$$C_r(\rho) = S[\Delta(\rho)] - S(\rho), \quad (\text{A6})$$

where Δ denotes the dephasing operation in the incoherent basis, and $S(\rho)$ denotes the von Neumann entropy of a quantum state ρ ,

$$S(\rho) = -\text{Tr}(\rho \log_2 \rho). \quad (\text{A7})$$

The REC has operational significance as it equals the *distillable coherence* (DC) C_d [10].

Regarding the quantification of coherence on one subsystem in a bipartite system, the *quantum-incoherent relative entropy of coherence* (QI REC) is defined as [54]

$$C_r^{A|B}(\rho^{AB}) = \min_{\chi^{A|B} \in \mathcal{I}^{A|B}} S(\rho^{AB} \| \chi^{A|B}), \quad (\text{A8})$$

where the minimum is taken over the set of QI states. The QI REC $C_r^{A|B}$ captures how close a quantum state is from the set of QI states. Another expression is [54]

$$C_r^{A|B}(\rho^{AB}) = S[\Delta^B(\rho^{AB})] - S(\rho^{AB}), \quad (\text{A9})$$

where Δ^B denotes dephasing in the incoherent basis of Bob.

3. Free operations in the resource theory of quantum coherence

The free operations in the QRT of coherence in a single system are operations that do not create coherence from incoherent states,

$$\Lambda(\rho) \in \mathcal{I}, \quad \forall \rho \in \mathcal{I}, \quad (\text{A10})$$

where \mathcal{I} denotes the set of incoherent states. Such operations constitute the largest possible set that are free and referred to as *maximally incoherent operations*. One subset of such free operations are incoherent operations, which were first introduced in [7], specified by a set of Kraus operators $\{K_n\}$, satisfying that each of its Kraus operators is incoherent,

$$K_n \mathcal{I} K_n^\dagger \subset \mathcal{I}^*, \quad \forall n, \quad (\text{A11})$$

where \mathcal{I}^* denotes the set of diagonal semi-definite Hermitian operators. A general *completely positive and trace preserving* (CPTP) map Λ is incoherent if there exists at least one incoherent Kraus representation. Then the *dephasing-covariant incoherent operations* (DIO) are maps Λ which commute with the dephasing operation Δ , i.e., $\Delta[\Lambda(\rho)] = \Lambda[\Delta(\rho)]$. And finally, the *strictly incoherent operations* form the smallest set of free operations, where both K_n and K_n^\dagger are incoherent operators.

Regarding the resource theory of coherence in a bipartite scenario, where the coherence of one subsystem is viewed as resource, the *local quantum-incoherent operations and classical communications* (LQICC) protocol was first introduced in [54]. In a bipartite system involving Alice and Bob, Bob is restricted to perform only local incoherent operations while Alice can perform arbitrary quantum operations on her system. Classical communications between them are allowed. The QI REC has the operational meaning that it upper bounds the optimal generation rate of the maximally coherent state $|\Phi_2\rangle$ on Bob's side in the LQICC protocol. The *distillable coherence of collaboration* (DCC) was first introduced in [54],

$$C_d^{A|B}(\rho^{AB}) = \sup \left\{ R : \lim_{n \rightarrow \infty} \left(\inf_{\Lambda} \|\Lambda[(\rho^{AB})^{\otimes n}] - \Phi_2^{\otimes [Rn]}\| \right) = 0 \right\}, \quad (\text{A12})$$

where the infimum is taken over all LQICC operations Λ and $[x]$ returns the maximum integer no larger than x . The DCC is upper bounded by the QI REC. For pure states, $C_d^{A|B}(|\Phi^{AB}\rangle) = C_r^{A|B}(|\Phi^{AB}\rangle)$ [54].

4. Relation between the QI REC and the SIC

First we introduce a relation between the QI REC and the *steering induced coherence* (SIC).

Proposition 1—For a bipartite state ρ^{AB} , the SIC is upper bounded by the QI REC; i.e., we have

$$C_r^{A|B}(\rho^{AB}) \geq \bar{C}_r^B(\rho^{AB}). \quad (\text{A13})$$

Proof—Note that the QI REC can be expressed as

$$C_r^{A|B}(\rho^{AB}) = \min_{\chi^{A|B} \in \mathcal{I}^{A|B}} S(\rho^{AB} \| \chi^{A|B}) = S[\rho^{AB} \| \Delta^B(\rho^{AB})]. \quad (\text{A14})$$

Recall that the quantum relative entropy has many important properties, such that [59, 65]:

$$(a) \quad S[\Lambda(\rho)\|\Lambda(\sigma)] \leq S(\rho\|\sigma), \quad (\text{A15a})$$

$$(b) \quad \sum_i p_i S(K_i \rho K_i^\dagger / p_i \| K_i \sigma K_i^\dagger / q_i) \leq \sum_i S(K_i \rho K_i^\dagger \| K_i \sigma K_i^\dagger), \quad (\text{A15b})$$

$$(c) \quad S\left(\sum_i P_i \rho P_i \middle\| \sum_i P_i \sigma P_i\right) = \sum_i S(P_i \rho P_i \| P_i \sigma P_i), \quad (\text{A15c})$$

$$(d) \quad S(P_i \otimes \rho \| P_i \otimes \sigma) = S(\rho \| \sigma) \quad (\text{A15d})$$

where $p_i = \text{Tr}(K_i \rho K_i^\dagger)$, $q_i = \text{Tr}(K_i \sigma K_i^\dagger)$, and $\{P_i\}$ is a set of orthogonal projectors.

Note that $\{\mathbf{M}_n^A = |n\rangle\langle n|^A\}$ is a set of projectors on Alice's system, corresponding to the measurement outcome n . Thus with property (a) in Eq. (A15), we have

$$C_r^{A|B}(\rho^{AB}) = S[\rho^{AB}\|\Delta^B(\rho^{AB})] \geq S\left[\sum_n \mathbf{M}_n^A \rho^{AB} \mathbf{M}_n^A \middle\| \sum_n \mathbf{M}_n^A \Delta^B(\rho^{AB}) \mathbf{M}_n^A\right]. \quad (\text{A16})$$

Following (c) in Eq. (A15), if we denote $\delta_n^B = \langle n|\rho^{AB}|n\rangle$, $p_n = \text{Tr}(\delta_n^B)$, and $\rho_n^B = \frac{\delta_n^B}{p_n}$, we have

$$S\left[\sum_n \mathbf{M}_n^A \rho^{AB} \mathbf{M}_n^A \middle\| \sum_n \mathbf{M}_n^A \Delta^B(\rho^{AB}) \mathbf{M}_n^A\right] = \sum_n S[\mathbf{M}_n^A \otimes \delta_n^B \| \mathbf{M}_n^A \otimes \Delta^B(\delta_n^B)]. \quad (\text{A17})$$

Then with property (b) in Eq. (A15), we can obtain

$$\sum_n S[\mathbf{M}_n^A \otimes \delta_n^B \| \mathbf{M}_n^A \otimes \Delta^B(\delta_n^B)] = \sum_n S[\delta_n^B \| \Delta^B(\delta_n^B)] \geq \sum_n p_n S[\rho_n^B \| \Delta^B(\rho_n^B)] = \sum_n p_n C_r^B(\rho_n^B). \quad (\text{A18})$$

Note that $\sum_n C_r^B(\rho_n^B)$ is the average coherence that Bob can obtain with Alice's measurement choice $\{\mathbf{M}_n^A = |n\rangle\langle n|^A\}$ and classical communications. No matter what measurement Alice actually chooses, Bob will reach an average coherence no greater than $C_r^{A|B}(\rho^{AB})$. Hence, we have $C_r^{A|B}(\rho^{AB}) \geq \bar{C}_r^B(\rho^{AB})$.

5. Difference between the QI REC and the quantum correlations

Note that the QI REC is essentially different from the measures of quantum correlations. First, any state that is not quantum-incoherent has nonzero QI REC. The difference between the measures of quantum correlations and the QI REC is that the latter is basis-dependent. One of the most popular measures of quantum correlations is the *relative entropy of quantum discord* [66–68], defined as

$$D(\rho^{AB}) = \min_{\delta^{AB} \in CC} S(\rho^{AB}\|\delta^{AB}) \quad (\text{A19})$$

where CC denotes the set of *classical correlated states* that can be written in the form of the sum of projectors

$$\delta^{AB} = \sum_{k,l} p_{kl} |k\rangle\langle k|^A \otimes |l\rangle\langle l|^B. \quad (\text{A20})$$

Now consider a family of bipartite states

$$f^{AB} = \sum_{k,m} p_{km} |k\rangle\langle k|^A \otimes |m\rangle\langle m|^B, \quad (\text{A21})$$

where $|k\rangle^A$ is any orthonormal basis of Alice, and $|m\rangle^B$ is any orthonormal basis of Bob that is not incoherent. Obviously, f^{AB} is not quantum-incoherent and thus has a nonzero QI REC, while f^{AB} has zero discord or entanglement. Moreover, we can also construct states that are quantum-incoherent but have nonzero quantum discord.

6. Concurrence

The concurrence is an entanglement monotone, defined for a mixed state of two qubits as:

$$E_c^{AB}(\rho) \equiv \max(0, \lambda_1 - \lambda_2 - \lambda_3 - \lambda_4), \quad (\text{A22})$$

where $\lambda_1, \dots, \lambda_4$ are the eigenvalues of the Hermitian matrix $R = \sqrt{\sqrt{\rho}\tilde{\rho}\sqrt{\rho}}$, with

$$\tilde{\rho} = (\sigma_y \otimes \sigma_y)\rho^*(\sigma_y \otimes \sigma_y), \quad (\text{A23})$$

where ρ^* denotes the spin-flipped state of ρ , σ_y a Pauli spin matrix, and the eigenvalues are listed in decreasing order.

Appendix B: Dynamical behaviors of the information carriers based on coherence in open systems

We first show that both the behaviors of the local coherence (of a single system) and the extended coherence (of the system and an ancilla) are monotonic under *incoherent open system dynamics* (IOSD).

A theoretical work [45] showed that CP-nondisvisibility of non-Markovian dynamics and monotonic behaviors of quantum coherence measures under *incoherent completely positive and trace preserving* (ICPTP) maps can be used to detect and quantify the non-Markovianity of an IOSD. Obviously the REC behaves monotonically in an IOSD.

Lemma 1—The amount of REC of a quantum system decreases monotonically in an IOSD $\{\Lambda_t\}$; i.e., for any $t \geq s \geq 0$, we have

$$C_r[\Lambda_t(\rho)] \leq C_r[\Lambda_s(\rho)]. \quad (\text{B1})$$

Proof—The family of IOSDs will preserve incoherent states; i.e., for each $\rho \in \mathcal{I}$, we have

$$\Lambda_t(\rho) \in \mathcal{I}, \quad (\text{B2})$$

for any $t \geq 0$. Let us denote the quantum states after evolution time s and t ($0 \leq s \leq t$) are ρ_s and ρ_t . Then the REC of ρ_t and ρ_s can be evaluated as

$$C_r(\rho_t) = S[\rho_t|\Delta(\rho_t)], \quad (\text{B3a})$$

$$C_r(\rho_s) = S[\rho_s|\Delta(\rho_s)]. \quad (\text{B3b})$$

Note that if $\{\Lambda_t\}$ is Markovian, we have $\Lambda_t = \Lambda_{t,s}\Lambda_{s,0}$, and $\Lambda_{t,s}$ is CPTP. Hence, we can use the relation

$$S[\rho_t|\Delta(\rho_t)] \leq S[\Lambda_{t,s}(\rho_s)|\Lambda_{t,s}\Delta(\rho_s)], \quad (\text{B4})$$

and the definition of coherence measure yields

$$C_r(\rho_t) = \min_{\delta_t \in \mathcal{I}} S(\rho_t|\delta_t) \leq S[\rho_t|\Lambda_{t,s}\Delta(\rho_s)]. \quad (\text{B5})$$

Then we can obtain

$$C_r(\rho_t) \leq S[\Lambda_{t,s}(\rho_s)|\Lambda_{t,s}\Delta(\rho_s)] \leq C_r(\rho_s). \quad (\text{B6})$$

We have also used the property in Eq. (A15) that the quantum relative entropy is contractive under CPTP maps. Thus we complete the proof.

When considering the overall coherence of the open system and an ancilla, we can obtain a similar conclusion. The theoretical work in [43] proposed an alternative non-Markovianity measure based on the REC, which uses the whole coherence in an extended Hilbert space (which is referred to as extended coherence) constituted by both the open system and its ancilla. They find that the proposed measure can capture effectively the characteristics of non-Markovianity of incoherent open quantum processes, including both the phase-damping channel and the amplitude-damping channel.

Lemma 2—The amount of extended coherence of the open system (Alice) and an ancilla (Bob) decreases monotonically in an IOSD $\{\Lambda_t^A\}$ on Alice; i.e., for any $t \geq s \geq 0$, we have

$$C_r[(\Lambda_t^A \otimes \mathbb{I}^B)(\rho_0^{AB})] \leq C_r[(\Lambda_s^A \otimes \mathbb{I}^B)(\rho_0^{AB})]. \quad (\text{B7})$$

Proof—Following [43] and the proof of *Lemma 1*, with

$$C_r(\rho_t^{AB}) = S[\rho_t^{AB} \|\Delta^{AB}(\rho_t^{AB})], \quad (\text{B8a})$$

$$C_r(\rho_s^{AB}) = S[\rho_s^{AB} \|\Delta^{AB}(\rho_s^{AB})], \quad (\text{B8b})$$

we have

$$C_r(\rho_t^{AB}) \leq S[\Lambda_{t,s}^A(\rho_s^{AB}) \|\Lambda_{t,s}^A \Delta^{AB}(\rho_s^{AB})] \leq C_r(\rho_s^{AB}). \quad (\text{B9})$$

Thus we see the dynamical behavior of the extended coherence during an IOSD.

From the above two Lemmas, we can see that both the coherence of the open system and the extended coherence of the open system and the ancilla decrease monotonically during an IOSD, and they can be used for efficiently detecting non-Markovianity in IOSDs. However, there are dynamics that are not incoherent. Hence, both of these information carriers will not decrease monotonically in these processes. We then prove *Theorem 1*, showing the monotonic behaviors of the *QI* REC during general open system dynamics.

Proof of Theorem 1—First we prove that the *QI* REC decreases monotonically during a Markovian evolution on Alice. The quantum states (initially ρ^{AB}) after evolution time s and t ($0 \leq s \leq t$) are ρ_s^{AB} and ρ_t^{AB} . We can express the *QI* REC as follows,

$$C_r^{A|B}(\rho_t^{AB}) = S[\rho_t^{AB} \|\Delta^B(\rho_t^{AB})] = S[\Lambda_{t,s}^A(\rho_s^{AB}) \|\Delta^B \Lambda_{t,s}^A(\rho_s^{AB})]. \quad (\text{B10})$$

As Δ^B acts only on B , and $\Lambda_{t,s}^A$ acts only on A , we have

$$\Delta^B \Lambda_{t,s}^A(\cdot) = \Lambda_{t,s}^A \Delta^B(\cdot). \quad (\text{B11})$$

Combining the contractive property, if the intermediate map $\Lambda_{t,s}^A$ is CP, we have

$$S[\rho_t^{AB} \|\Delta^B(\rho_t^{AB})] \leq S[\rho_s^{AB} \|\Delta^B(\rho_s^{AB})]. \quad (\text{B12})$$

Thus during a Markovian process, the *QI* REC decreases monotonically.

Then we prove that the SIC decreases monotonically during a Markovian evolution on Alice. It is well known that any CPTP operation on Alice can be constructed by first implementing a unitary U to A and an ancilla A' , then discarding A' . The corresponding mathematical formulation can be described by

$$\Lambda(\rho^A) = \text{Tr}_{A'}[U(\rho^A \otimes \rho^{A'})U^\dagger], \quad (\text{B13})$$

where ρ^A and $\rho^{A'}$ denote the quantum states of A and A' .

Note that if Bob shares a multipartite state $\rho^{A_1 \dots A_n B}$ made of n parties A_1, A_n, \dots, A_n , the generalized steering-induced coherence can be expressed as

$$\bar{C}_r^B(\rho^{A_1 \dots A_n B}) = \max_{\mathcal{M}_{A_1 \dots A_n}} \sum_m p_m C_r(\rho_m^B), \quad (\text{B14})$$

where $\mathcal{M}_{A_1 \dots A_n}$ denotes the collective projective measurements across n particles. In our case, Alice (A), Bob and the ancilla A' share a tripartite state before the unitary U , where A and A' are uncorrelated. The overall state admits the form

$$\rho^{A'AB} = \rho^{A'} \otimes \rho^{AB}. \quad (\text{B15})$$

As the collective measurement on A and A' will reduce to a *positive-operator valued measure* (POVM) on A , and the set of all POVMs on A forms a strict larger set than the set of all local projective measurements, yielding higher average coherence that can be obtained on Bob's system in general. Thus, we obtain the following relation,

$$\bar{C}_r^B(\rho^{A'AB}) = \max_{\mathcal{M}_{AA'}} \sum_m p_m C_r(\rho_m^B) \geq \bar{C}_r^B(\rho^{AB}). \quad (\text{B16})$$

The above inequality is valid in a more general case when A and A' are correlated. However, in the case when A' and A are product states, we have

$$\bar{C}_r^B(\rho^{A'AB}) = \bar{C}_r^B(\rho^{AB}). \quad (\text{B17})$$

First we present the proof of this statement. Considering a projective collective measurement, specified by

$$\{\mathcal{M}_{A'A}^k = |\psi_k\rangle\langle\psi_k|\}, \quad (\text{B18})$$

which acts on A and A' , where $\{|\psi_k\rangle\}$ forms a set of orthogonal normalized bases of the overall system,

$$|\psi_k\rangle = \sum_{a,a'} \sqrt{r_{aa'}^k} |a'\rangle \otimes |a\rangle. \quad (\text{B19})$$

Here $\{|a'\rangle\}$ and $\{|a\rangle\}$ are a set of orthonormal bases on A' and A , respectively, and the normalization condition leads to

$$\sum_{a,a'} r_{aa'}^k = 1. \quad (\text{B20})$$

The reduced POVM on A reads

$$M_k = \sum_{a,a'} r_{aa'}^k \langle a' | \rho^{A'} | a' \rangle |a\rangle\langle a|, \quad (\text{B21})$$

which corresponds to the auxiliary state $\rho^{A'}$. The complete condition for POVM requires that

$$\sum_k M_k = \mathbb{I}, \quad (\text{B22})$$

where \mathbb{I} denotes the identity operator on A . Using the relation $\sum |a\rangle\langle a| = \mathbb{I}$, we have

$$\sum_{k,a'} r_{aa'}^k \langle a' | \rho^{A'} | a' \rangle = 1. \quad (\text{B23})$$

Then after implementing the POVM, Bob can obtain the state from Alice's outcome m_k according to each M_k . The state of Bob can be expressed as

$$\rho_k^B = \frac{\text{Tr}_A(M_k \rho^{AB})}{\text{Tr}_{AB}(M_k \rho^{AB})}. \quad (\text{B24})$$

Denoting $p_k = \text{Tr}_{AB}(M_k \rho^{AB})$, the average coherence obtained by Bob after the implementation of the POVM can be expressed as

$$\bar{C}_r^B(\rho^{A'AB} | M_{A'A}) = \sum_k p_k C_r(\rho_k^B). \quad (\text{B25})$$

If we denote the state ρ_a^B as Bob's state after Alice's projective measurement $|a\rangle$, then we have

$$\rho_k^B = \frac{1}{p_k} \sum_{a,a'} r_{aa'}^k \langle a' | \rho^{A'} | a' \rangle p_a \rho_a^B, \quad (\text{B26})$$

where $p_a = \text{Tr}(|a\rangle\langle a| \rho^{AB})$. Then the average coherence becomes

$$\bar{C}_r^B(\rho^{A'AB} | M_{A'A}) = \sum_k p_k C_r \left(\frac{1}{p_k} \sum_{a,a'} r_{aa'}^k \langle a' | \rho^{A'} | a' \rangle p_a \rho_a^B \right). \quad (\text{B27})$$

As the convexity of REC [7],

$$C_r \left(\sum_i p_i \rho_i \right) \leq \sum_i p_i C_r(\rho_i), \quad (\text{B28})$$

the REC will not increase under mixture of quantum states,

$$\sum_k p_k C_r \left(\frac{1}{p_k} \sum_{a,a'} r_{aa'}^k \langle a' | \rho^{A'} | a' \rangle p_a \rho_a^B \right) \leq \sum_{a,a',k} r_{aa'}^k \langle a' | \rho^{A'} | a' \rangle p_a C_r(\rho_a^B). \quad (\text{B29})$$

Combining Eq. (B22) and Eq. (B23), we have

$$\sum_{a,a',k} r_{aa'}^k \langle a' | \rho^{A'} | a' \rangle p_a C_r(\rho_a^B) = \sum_a p_a C_r(\rho_a^B), \quad (\text{B30})$$

the right hand of inequality (B30) is the average coherence, obtained by the projective measurement $\{|a\rangle\langle a|\}$ on A . From the inequality we can see that the average coherence, obtained from any collective projective measurement on A' and A , is no greater than the average coherence, which is obtained from a proper projective measurement on A if A and A' are product states. After the CPTP operations on A , which is realized by the unitary on A' and A , the maximum of average coherence obtained from the collective projective measurement remains unchanged, i.e.,

$$\bar{C}_r^B(\rho^{A'AB}) = \bar{C}_r^B(\rho_U^{A'AB}), \quad (\text{B31})$$

where $\rho_U^{A'AB} = U^{AA'} \rho^{A'AB} (U^{AA'})^\dagger$. The average coherence obtained from the collective projective measurement on A and A' is upper bounded by $\bar{C}_r^B(\rho^{AB})$. After the unitary U , we have

$$\bar{C}_r^B(\rho_U^{A'AB}) = \bar{C}_r^B(\rho^{AB}). \quad (\text{B32})$$

When tracing over A' , the set of projective measurements on A is a strict subset of the reduced POVMs corresponding to collective projective measurements on A and A' . Thus, we have

$$\bar{C}_r^B(\rho_U^{AB}) \leq \bar{C}_r^B(\rho_U^{A'AB}), \quad (\text{B33})$$

where ρ_U^{AB} denotes the final states of Alice and Bob after the implementation of U ,

$$\rho_U^{AB} = \text{Tr}_{A'}(\rho_U^{A'AB}). \quad (\text{B34})$$

Using the fact that any CPTP map on A can be constructed by unitary interaction between A and an uncorrelated A' , as denoted in Eq. (B13), the SIC of B will decrease under a CPTP map on A ,

$$\bar{C}_r^B[\Lambda^A(\rho^{AB})] \leq \bar{C}_r^B(\rho^{AB}). \quad (\text{B35})$$

Thus we complete the proof. This result shows that the Markovianity on Alice's evolution will reduce the steerability of Alice to Bob's state, shrinking the accessible states of Bob, while the local state of Bob ρ^B will remain unchanged.

Appendix C: Numerical simulations for different processes

In this section we present the numerical simulations to show the behaviors of the local coherence of a single system, the extended coherence with an ancilla, the QI REC, and the SIC, under different non-Markovian quantum dynamics. To simulate the behavior of the REC of a single qubit system, we use the initial pure state

$$|\psi_0\rangle^A = \frac{1}{2} (\sqrt{3}|0\rangle + |1\rangle). \quad (\text{C1})$$

And to simulate the dynamical behaviors of the extended coherence with an ancilla, the QI REC, and the SIC on a bipartite system, we choose the initial two-qubit entangled state

$$|\psi_0\rangle^{AB} = \frac{1}{4} (\sqrt{6}|00\rangle + \sqrt{2}|01\rangle + \sqrt{2}|10\rangle + \sqrt{6}|11\rangle). \quad (\text{C2})$$

We consider two kinds of quantum dynamics: the amplitude-damping channels and the multiple decoherence channels.

1. Amplitude-damping channels

We now consider the single-qubit amplitude-damping channels modeled by the Hamiltonian

$$H_{\text{tot}} = \frac{1}{2}\omega_0\sigma_z + \sum_i \omega_i a_i^\dagger a_i + \sum_i (g_i \sigma_+ a_i + g_i^* \sigma_- a_i^\dagger) \quad (\text{C3})$$

where, σ_+ and σ_- are the raising and lowering operators for the qubit. The master equation corresponding to the Hamiltonian in Eq. (C3) is given by

$$\frac{d}{dt}\rho_t = -\frac{i}{4}S(t)[\sigma_z, \rho] + \gamma(t)\left(\sigma_- \rho_t \sigma_+ - \frac{1}{2}\{\sigma_+ \rho_t \sigma_- - \rho_t\}\right) \quad (\text{C4})$$

where the quantities $S(t)$ and $\gamma(t)$ read

$$S(t) = -2\text{Im}\frac{\dot{G}(t)}{G(t)}, \quad (\text{C5a})$$

$$\gamma(t) = -2\text{Re}\frac{\dot{G}(t)}{G(t)}, \quad (\text{C5b})$$

and the decoherence function $G(t)$ depends on the spectral density $J(\omega)$. Considering a Lorentzian shape spectral density,

$$J(\omega) = \frac{\gamma_0 \lambda^2}{[(\omega_0 + \delta - \omega)^2 + \lambda^2]}, \quad (\text{C6})$$

and letting $\delta = 0$, one obtains the decoherence function $G(t)$ as

$$G(t) = \exp\left(\frac{-\lambda t}{2}\right) \left[\cosh\left(\frac{dt}{2}\right) + \frac{\lambda}{d} \sinh\left(\frac{dt}{2}\right) \right] \quad (\text{C7})$$

where $d = \sqrt{\lambda^2 - 2\gamma_0\lambda}$.

Here, we consider both Markovian dynamics (when $\gamma_0 < \lambda/2$), and non-Markovian dynamics (when $\gamma_0 > \lambda/2$). The corresponding results are shown in Fig. 6 and Fig. 7, respectively.

In the Markovian regime, we choose $\gamma_0 = 0.2\lambda$, the dynamical behaviors of the QI REC, the extended coherence, and the local coherence, with respect to different bases (as shown in Fig. 6). We simulate the dynamical behaviors of the above coherence measures in different reference bases. In the Markovian regime of the amplitude-damping channels, the QI REC and the extended coherence behaves monotonically. However, the local coherence behaves differently in different reference bases; i.e., the monotonicity depends on the choice of reference basis. Note that although the extended coherence of Alice and Bob behaves monotonically in all reference bases in the Markovian regime of the amplitude-damping channel, it cannot be used for detecting non-Markovianity in the general evolution as the case we have experimentally shown in the main text.

In the non-Markovian regime, we choose $\gamma_0 = 25\lambda$, resulting in the non-Markovianity of the open system dynamics. In this case, we simulate both the QI REC and the SIC with respect to different bases (as shown in Fig. 7). From the simulation, we can see that during the amplitude-damping channel, the non-Markovianity can be detected with both the QI REC and the SIC (note that in the above case the values of the SIC are coincident in all reference bases) independent of the reference basis we choose.

2. Multiple decoherence channels

The dynamics of a single qubit in multiple decoherence channels can be considered for a two-level system with the master equation

$$\frac{d}{dt}\rho_t = \frac{1}{2} \sum_{i=1}^3 \gamma_i(t)(\sigma_i \rho_t \sigma_i - \rho_t), \quad (\text{C8})$$

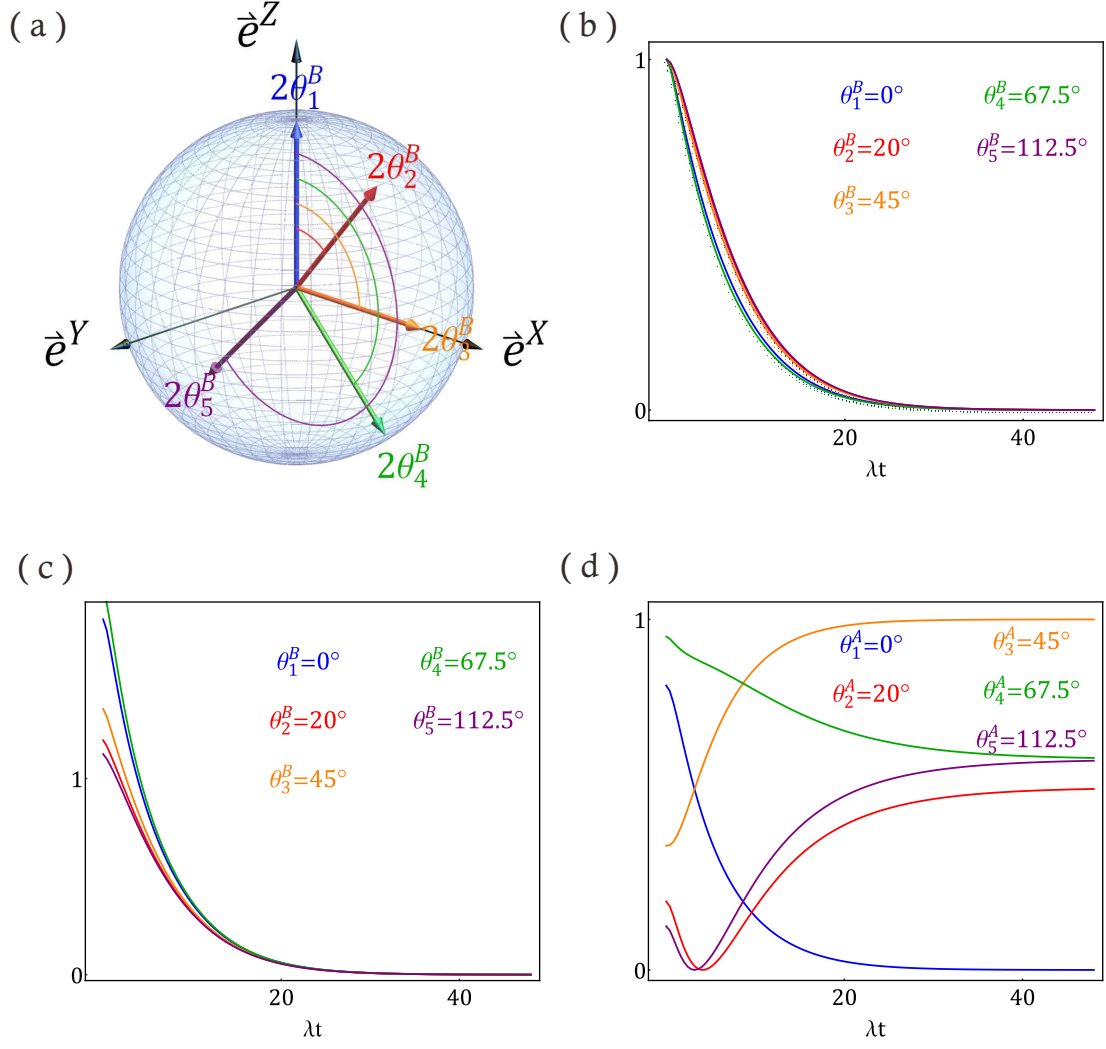


Figure 6. **Theoretical simulations for the Markovian amplitude-damping channels.** In the Markovian regime, the simulations of the dynamical behaviors of the QI REC (b), the extended coherence (c), and the local coherence (d) are shown. The reference bases of Alice (Bob) are chosen as the eigenbasis of $\sigma \cdot \mathbf{n}[\theta_i^{A(B)}]$ with different $\theta_i^{A(B)}$, where $\mathbf{n}(\theta_i^B) = \sin 2\theta_i^B \mathbf{e}^X + \cos 2\theta_i^B \mathbf{e}^Z$. During the Markovian evolution, when $\gamma_0 = 0.2\lambda$, both the QI REC and the extended coherence of ρ^{AB} decrease monotonically. The dynamical behavior of the local coherence of A is non-monotonic and depends on the basis we choose.

where σ_i denotes the i th Pauli matrix. The dynamical map corresponding to Eq. (C8) can be exactly worked out and is given by the random unitary dynamics

$$\Lambda_i(\rho) = \sum_{i=0}^3 p_i(t) \sigma_i \rho \sigma_i. \quad (\text{C9})$$

Here, for the Markovian dynamics, we set the parameters $\gamma_i(t)$ as follows

$$\gamma_1(t) = \gamma_2(t) = \gamma_3(t) = \frac{c}{2}, \quad (\text{C10})$$

and for the non-Markovian dynamics, we set the aforementioned parameters as

$$\gamma_1(t) = \gamma_2(t) = \frac{c}{2}, \quad (\text{C11a})$$

$$\gamma_3(t) = \frac{c\lambda \cos ct}{2}, \quad (\text{C11b})$$

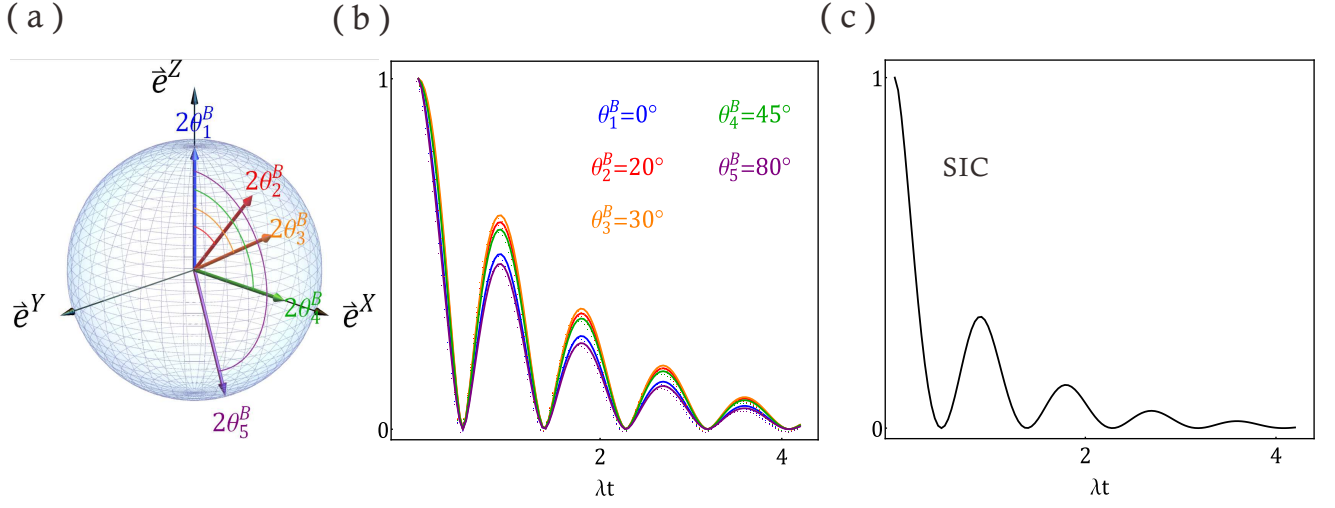


Figure 7. **Theoretical simulations for the non-Markovian amplitude-damping channels.** In the non-Markovian regime, $\gamma_0 = 25\lambda$, the non-Markovianity can be captured by the QI REC (b) and the SIC (c), where the SIC behaves exactly the same in all reference bases, chosen as the eigenbasis of $\sigma \cdot \mathbf{n}(\theta_i^B)$ with different θ_i^B , where $\mathbf{n}(\theta_i^B) = \sin 2\theta_i^B \mathbf{e}^X + \cos 2\theta_i^B \mathbf{e}^Z$.

where $c > 0$, and $\lambda > 0$, controlling the degree of non-Markovianity.

In the Markovian regime, the dynamics of the system can be exactly solved as

$$p_0(t) = \frac{1 + 3 \exp(-2ct)}{4}, \quad (\text{C12a})$$

$$p_1(t) = p_2(t) = p_3(t) = \frac{1 - \exp(-2ct)}{4}. \quad (\text{C12b})$$

The numerical simulations of the dynamical behaviors of the QI REC, the extended coherence, and the local coherence, with respect to different bases (as shown in Fig. 8). In this case, all the above coherence measures behave monotonically during the Markovian dynamics.

In the non-Markovian regime, the dynamics of the system can be solved as

$$p_0(t) = \frac{1 + \exp(-2ct) + 2 \exp(-ct - \lambda \sin ct)}{4}, \quad (\text{C13a})$$

$$p_1(t) = p_2(t) = \frac{1 - \exp(-2ct)}{4}, \quad (\text{C13b})$$

$$p_3(t) = \frac{1 + \exp(-2ct) - 2 \exp(-ct - \lambda \sin ct)}{4}. \quad (\text{C13c})$$

We set $\lambda = 3.8$. The dynamical behaviors of the QI REC, and the SIC are simulated with respect to different bases, as shown in Fig. 9. We can see that in all reference bases chosen, the non-Markovianity can be captured by both the temporal increase of the QI REC and the SIC.

Appendix D: Non-Markovianity measure based on the QI REC

In this section, we define a new method for non-Markovianity measure based on the QI REC, which is

$$\mathcal{N}_{QI}(\Lambda) = \max_{|i\rangle^B} \int_{\sigma > 0} \sigma(t, |i\rangle^B), \quad (\text{D1})$$

where

$$\sigma(t, |i\rangle^B) = \frac{\partial C_r^{A|B_i}}{\partial t} [\Lambda \otimes \mathbb{I}(|\Phi\rangle\langle\Phi|)], \quad (\text{D2})$$

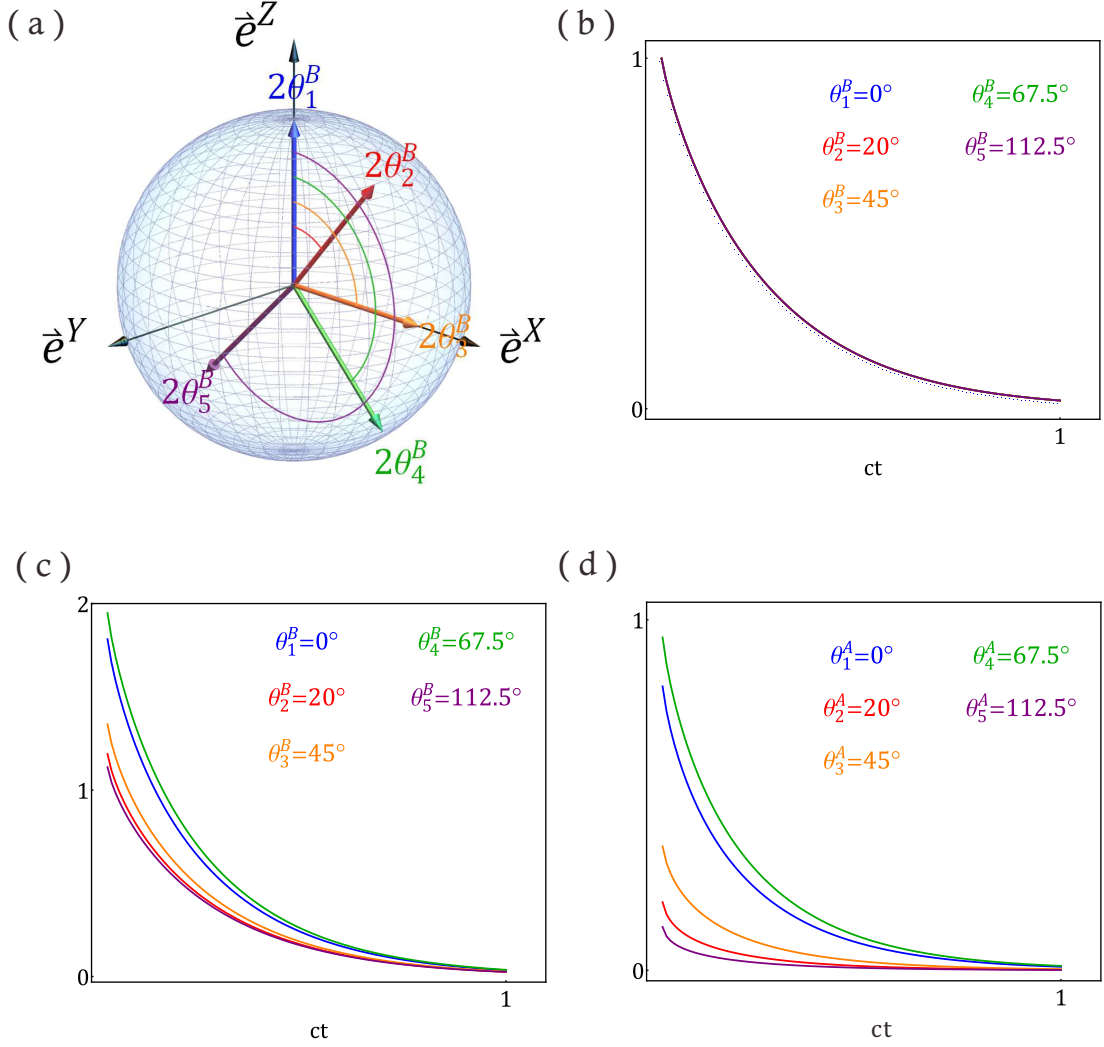


Figure 8. **Theoretical simulations for the Markovian multiple decoherence channels.** In the Markovian regime, the numerical simulations of the dynamical behaviors of the QI REC (b), the extended coherence (c), and the local coherence (d) are shown. The reference basis of Alice (Bob) is chosen as the eigenbasis of $\sigma \cdot \mathbf{n}[\theta_i^{A(B)}]$ with different $\theta_i^{A(B)}$, where $\mathbf{n}(\theta_i) = \sin 2\theta_i^B \mathbf{e}^X + \cos 2\theta_i^B \mathbf{e}^Z$. In the Markovian regime, all information quantifiers behave monotonically independent of the basis chosen.

$C_r^{A|B_i}$ denotes the QI REC with respect to the reference basis $\{|i\rangle^B\}$ of Bob, and $|\Phi\rangle$ can be any pure bipartite maximally entangled state. Thus, this definition only needs optimization over all local bases of Bob's system.

In order to figure out the property of this non-Markovianity measure, let us first recall two popular non-Markovian measures. One was defined by Breuer, Laine, and Piilo (BLP) [29]. A dynamical map $\{\Lambda_t\}$ is Markovian if the distinguishability of any two evolving quantum states ρ and τ decreases, and the associated measure for non-Markovianity measure is then defined as

$$\mathcal{N}_{\text{BLP}} = \max_{\rho, \tau} \int_{(\partial\|\rho_t - \tau_t\|/\partial t) > 0} \frac{\partial\|\rho_t - \tau_t\|}{\partial t} dt. \quad (\text{D3})$$

Here ρ and τ denote the initial pairs of quantum states, and $\|\cdot\|$ denotes the trace distance. However, this involves a formidable optimization over all pairs of density operators, which is relatively harder to carry out when working with a high-dimensional system.

The other one was proposed by Rivas, Huelga, and Plenio (RHP) in [30]:

$$\mathcal{N}_{\text{RHP}} = \int_0^\infty \lim_{\varepsilon \rightarrow 0} \frac{\text{Tr}[\Lambda_{t+\varepsilon, t} \otimes \mathbb{I}(|\Phi\rangle\langle\Phi|)] - 1}{\varepsilon} dt \quad (\text{D4})$$

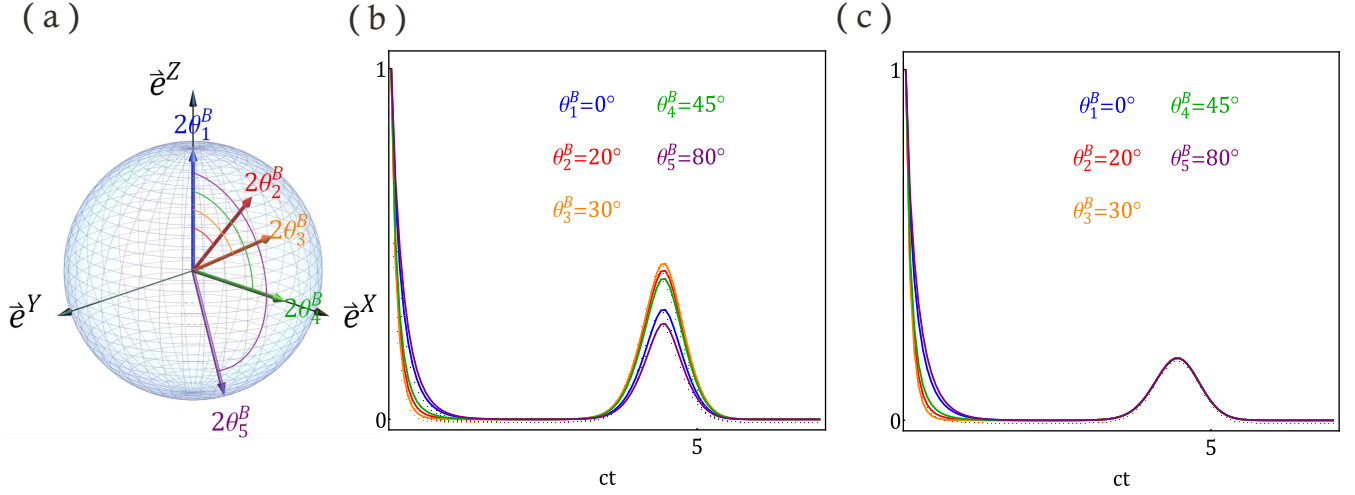


Figure 9. **Theoretical simulations for the non-Markovian multiple decoherence channels.** In the non-Markovian regime, the non-Markovianity can be simultaneously captured by the temporal increase of the *QI REC* (b) and the *SIC* (c), in all reference bases of Bob, chosen as the eigenbasis of $\sigma \cdot \mathbf{n}(\theta_i^B)$ with different θ_i^B , where $\mathbf{n}(\theta_i^B) = \sin 2\theta_i^B \mathbf{e}^X + \cos 2\theta_i^B \mathbf{e}^Z$.

where $|\Phi\rangle$ denotes a maximally entangled state shared by the open system and ancilla. However, this approach needs the computation of the transition map $\Lambda_{t+\varepsilon,t}$, which cannot be evaluated in general. Moreover, an entanglement measure is often difficult to evaluate itself especially in a high-dimensional system.

Appendix E: Experimental aspects

1. State preparation

In the state preparation module (I), two type-I phase-matched β -barium borate (BBO) crystals, whose optical axes are normal to each other, are pumped by a continuous-wave Ar^+ laser at 351.1 nm, with a power of around 50 mW, for the generation of photon pairs with a central wavelength at $\lambda=702.2$ nm via a *spontaneous parametric down-conversion process* (SPDC). A half-wave plate working at 351.1 nm set before the lens and BBO crystals is used to control the polarization of the pump laser. The two polarization-entangled photons are then separately distributed through two single-mode fibers (SMF), where one represents Bob and the other Alice. Two interference filters with a 4 nm *full width at half maximum* (FWHM) are placed to filter out proper transmission peaks. HWPs at both ends of the SMFs are used to control the polarization of both photons. A quarter-wave plate in Bob's arm is used to compensate the phase for the desired prepared state. A Fabry-Pérot cavity which is 0.06 mm thick and coated with a partial reflecting coating on each side at 702.2 nm (actually the experimental accessible FP cavity is coated with a reflectivity of around 0.85 of both sides at 780 nm, which is close to the value of the reflectivity at 702.2 nm) can be inserted into Alice's arm to change her initial environment. The setup can generate arbitrary pure bipartite states

$$|\Psi^{AB}\rangle = |\psi(\theta)\rangle^{AB} \otimes |\chi\rangle^A, \quad (\text{E1})$$

where $|\psi(\theta)\rangle^{AB}$ denotes the entangled pure states shared by Alice and Bob,

$$|\psi(\theta)\rangle^{AB} = \cos 2\theta|00\rangle + \sin 2\theta|11\rangle, \quad (\text{E2})$$

with arbitrary tunable θ , and $0 \equiv H$, $1 \equiv V$, representing an incoherent basis. The maximally entangled state $|\psi(\frac{\pi}{8})\rangle$ can be prepared with a fidelity of 0.985, with an interference visibility $C_{DD} : C_{DA} \geq 100$, where C_{DD} (C_{DA}) denotes coincident events when Alice is in the state $|D\rangle = \frac{1}{\sqrt{2}}(|0\rangle + |1\rangle)$ and Bob is in the state $|D\rangle$ [$|A\rangle = \frac{1}{\sqrt{2}}(|0\rangle - |1\rangle)$]. The environmental state can be expressed as

$$|\chi\rangle^A = \int \mathbf{d}\omega f(\omega)|\omega\rangle, \quad (\text{E3})$$

which involves the amplitude $f(\omega)$ for Alice's photon in a mode with frequency ω [57].

2. Evolution

In the evolution module (II), all plates (QPs, QWPs and HWPs) are mounted on rotation frames that allow us to construct a dephasing process in an arbitrary orthogonal basis,

$$|n_+(\alpha)\rangle = \cos \alpha |0\rangle + \sin \alpha |1\rangle, \quad (\text{E4a})$$

$$|n_-(\alpha)\rangle = -\sin \alpha |0\rangle + \cos \alpha |1\rangle, \quad (\text{E4b})$$

where α depends on the angle of the optical axis of the QPs. A QWP (rotation angle set to α) in Alice's arm is used for phase compensation between the $|n_+(\alpha)\rangle$ and $|n_-(\alpha)\rangle$ polarized photons. The experimental evolution admits a simple theoretical analysis which is described by a unitary transformation

$$|n_\pm(\alpha)\rangle \otimes |\omega\rangle \xrightarrow{U(\alpha)} \exp(-in_\pm \omega t) |n_\pm(\alpha)\rangle \otimes |\omega\rangle; \quad (\text{E5})$$

the corresponding dynamical map Λ_t takes the form,

$$|n_+(\alpha)\rangle\langle n_+(\alpha)| \xrightarrow{\Lambda_t} |n_+(\alpha)\rangle\langle n_+(\alpha)|, \quad (\text{E6a})$$

$$|n_-(\alpha)\rangle\langle n_-(\alpha)| \xrightarrow{\Lambda_t} |n_-(\alpha)\rangle\langle n_-(\alpha)|, \quad (\text{E6b})$$

$$|n_+(\alpha)\rangle\langle n_-(\alpha)| \xrightarrow{\Lambda_t} \kappa(t) |n_+(\alpha)\rangle\langle n_-(\alpha)|, \quad (\text{E6c})$$

$$|n_-(\alpha)\rangle\langle n_+(\alpha)| \xrightarrow{\Lambda_t} \kappa^*(t) |n_-(\alpha)\rangle\langle n_+(\alpha)|, \quad (\text{E6d})$$

where the decoherence factor reads

$$\kappa(t) = \int \mathbf{d}\omega |f(\omega)|^2 \exp(-i\Delta n \omega t), \quad (\text{E7})$$

and $\Delta n = n_+ - n_-$ denotes the nonzero difference in the refraction indices of the $|n_+(\alpha)\rangle$ and $|n_-(\alpha)\rangle$ polarized photons.

All theoretical simulations are performed considering the experimental imperfections, including the experimentally prepared quantum states. For simulating the two aforementioned processes, Λ_t^M and Λ_t^{NM} , for Markovian and non-Markovian dynamics, we have made the assumption that in the experiments of the Markovian process, the frequency distribution can be well described with a Gaussian profile with a standard deviation of 6.50×10^{12} Hz (its corresponding FWHM is 3.4 nm). While the non-Markovian process can be well modeled by a sum of two Gaussians centered at two different frequencies, corresponding to wavelengths 700.6 nm and 703.3 nm with amplitudes 0.65 and 0.35.

The essential difficulty in the experiments is the phase compensation for conducting the correct evolution. In the first part of the experiments, the Markovian evolution is constructed as pure dephasing in the eigenbasis $\{|n_+(20^\circ)\rangle, |n_-(20^\circ)\rangle\}$ of $\sigma \cdot \mathbf{n}_0$, where $\mathbf{n}_0 = \cos 40^\circ \mathbf{e}^X + \sin 40^\circ \mathbf{e}^Z$. Hence, we rotate all QPs to 20° . In ideal case, we assume that no additional phase is introduced between $|n_+(20^\circ)\rangle$ and $|n_-(20^\circ)\rangle$. However, in our experiments, an additional phase $\phi(t)$ will be introduced and the evolution of the extended coherence and the local coherence will behave differently depending on the additional phase $\phi(t)$. For solving this problem, we insert a QWP with rotation angle 20° to compensate the phase, removing $\phi(t)$. As we take experimental data using QPs with different lengths for each evolution time t , the phase compensation is performed each time when we change the lengths of the QPs. In the experiments with the non-Markovian process, since the dynamical behavior of neither the local coherence nor the extended coherence is taken into consideration, the additional phase will not play an important role in the experimental errors. Thus, the *QI* REC is more robust to phase errors in our protocols.

3. State tomography and coherence detection

In the detection module (III), the extinction ratio of the reflected arm of a PBS is lower than the transmissive arm. For improving the extinction ratio, we use a HWP with rotation angle set to 45° and another PBS placed in the reflected arm, resulting in an increase in the extinction ratio. Thus the precision of the tomography process can be improved.

We use multi-mode fibers for directing photons from the free space to the detectors. The use of multi-mode fibers can increase and stabilize the collection efficiency of the photons. The power of the 351.1 nm continuous laser is set to about 50 mW, and the coincidence window is set at 4 ns, resulting in around 1000 coincident events in one second.

The overall quantum state can be reconstructed via the combination of four wave plates (two HWPs and two QWPs) and two PBSs, performing a standard two-qubit state tomography. The state of a single system can also be

analyzed via two wave plates and one PBS on Alice's side, while Bob's photons are used as the trigger. Then the coherence-related measures can be calculated directly from the experimentally reconstructed quantum states $\tilde{\rho}$.
